Topology of Pretreated Wood Fibers Using Dynamic Nuclear Polarization

Jasmine Viger-Gravel,[†] Wu Lan,[†] Arthur C. Pinon,[†,‡] Pierrick Berruyer,[†] Lyndon Emsley,[†]
Michel Bardet,*[†,§] and Jeremy Luterbacher*[†]

[†]Institut des Sciences et Ingénierie Chimiques, Ecole Polytechnique Fédérale de Lausanne (EPFL), CH-1015 Lausanne, Switzerland

[‡]Department of Health Technology, Center for Hyperpolarization in Magnetic Resonance, Technical University of Denmark, Building 349, DK-2800 Kgs Lyngby, Denmark

[§]Univ. Grenoble Alpes, CEA, IRIG-MEM, Laboratoire de Résonance Magnétique, Grenoble 38000, France

S Supporting Information

ABSTRACT: In the continuously developing field of lignocellulosic biomass, high-yield lignin depolymerization processes are sought to optimize its productivity and profitability. Recently, formaldehyde stabilization during lignin extraction and biomass pretreatment has been found to drastically enhance subsequent lignin upgradeability but can affect cellulose digestibility. The exact role and/or form of formaldehyde on the residual biomass surface is still not fully understood. Here, we use magic angle spinning (MAS) dynamic nuclear polarization (DNP) methods to characterize the components that remain inside the residual cell wall after the lignin extraction process and reveal the topochemistry of the solid residue. The regioselectivity of relayed DNP allows the observation of hyperpolarization in a range of 40−200 nm from the surface of the cell wall for poplar wood materials. That regioselectivity allows us to distinguish between the external secondary cell wall and the inner middle lamellae. In that respect, for the untreated wood, we confirm that there is less lignin in the outer part of the cell wall than deeper inside. In treated wood, we determine that the role of dioxane during the process is to enable the extraction of the modified products from the cell wall. We show that the modified lignins which were not extracted in the absence of dioxane accumulate in a 40 nm region at the surface of the cell wall. Also, using carbon-13 enriched formaldehyde during the process, we show that 1% of the total amount of carbon in the material is assigned to self-polymerization and that no covalent bonds to cellulose are observed.
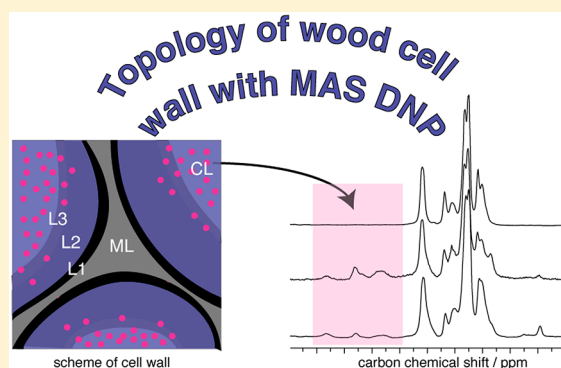
1. INTRODUCTION

Pretreatment (or delignification) is a key process in biorefineries and pulp and paper processes that facilitates integrated biomass utilization. This step fractionates the biomass into its three major components, cellulose, hemicelluloses, and lignin (see chemical structures in Scheme 1), facilitating downstream process with the objective of converting each component into value-added products.[1−4] Recently, a lignin extraction process using aliphatic aldehydes was developed that leads to in situ stabilization of the lignin structure during acid pretreatment, leaving behind a high purity cellulose-rich solid.[5−7] Despite its purity, this leftover solid still needed further acid treatment before enzymatic hydrolysis to release high yields of glucose when formaldehyde was used. The exceptional purity of the cellulose after treatment was thought to be due to the excellent solubilization of stabilized lignin in the chosen solvent system, which avoided recondensation or redeposition of the lignin on the solid surface. The reason for the need for an additional acid treatment was thought to be a reaction between the

formaldehyde and the hydroxyl on the cellulose surface, which could have prevented reaction between the cellulose and enzyme. However, no direct evidence showed that formaldehyde did react with the cellulose.[5] Here, we use magic angle spinning dynamic nuclear polarization (MAS DNP) NMR spectroscopy methods to illustrate the delignification process, reveal the topochemistry of the solid residue, and elucidate the exact nature of the components that remain inside the residual cell wall after the fractionation process.

High-resolution liquid-state NMR of either ^{1}H or ^{13}C have been used in this area for several decades and have provided data to elucidate the main polymer components of wood to better understand the chemistry and biochemistry of plant cell walls.[8−14] However, the acquisition of NMR spectra in solution requires the extraction of the key components, which leads to chemical modifications, and, by nature, destroys the spatial

Scheme 1[a]
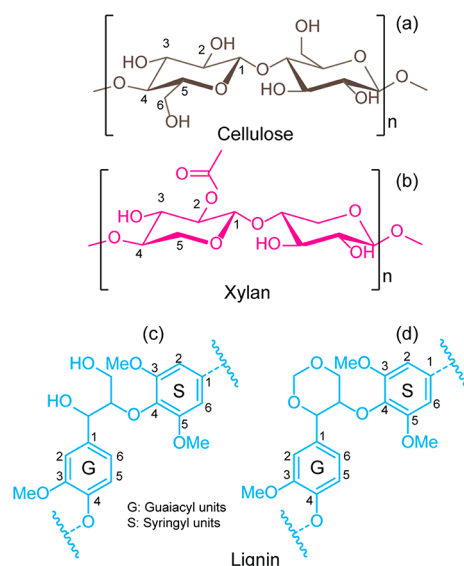
[a]Molecular structure of (a) cellulose, (b) Xylan, the most abundant chemical component of hemicellulose (the acetates are randomly distributed on the hemicelluloses and so do not necessarily repeat regularly), (c) lignin, and (d) formaldehyde stabilized lignin.

arrangement of the constituents. Gel-state NMR methods were developed to characterize whole cell wall biomass nondestructively but these methods require extensive preparation and cannot provide information on the surface functionalities of the biomass.[15,16] To circumvent this, high-resolution solid-state NMR has become the method of choice for the study of unmodified lignocellulosic samples, allowing the determination of the three-dimensional structure of polymers and their spatial localization inside cell walls, notably with high-resolution magic angle spinning (MAS) solid state ^{13}C NMR experiments.[17−26]

While detailed structural studies using multidimensional NMR often previously required ^{13}C enriched samples, the recent advent of dynamic nuclear polarization (DNP)[27] methods for MAS NMR of materials[28,29] has allowed the study of a wide variety of materials at natural isotopic abundance such as functionalized surfaces,[28−31] nanoparticles,[32,33] inorganic solids,[34,35] polymers,[36−49] or biomolecules.[50−55] MAS DNP techniques have also been recently applied to isolated celluloses, cellulose derivatives in pharmaceutical formulations,[56−59] modified lignocellulosic biomass, and functionalized paper substrates at natural abundance.[19,60−63]

MAS DNP experiments are usually carried out on powdered samples using the incipient wetness impregnation (IWI) technique,[28,29] which requires doping the sample with a source of unpaired electrons by impregnating the dry powder with a radical solution. The source of unpaired electrons is usually a solution containing a stable radical. The radicals most widely used today for cross effect DNP (currently the most efficient DNP mechanism at moderate magnetic field, e.g., 9.4 T, and at temperatures ∼ 100 K) include AMUPol,[64] TOTAPOL,[65] or TEKPol.[66,67] Irradiation of the NMR sample with microwaves to saturate the EPR transition of the unpaired electron can lead to spontaneous transfer of polarization from the electrons to the nearby nuclear spins, usually the protons of the frozen

solvent. The polarization is then further transferred to heteronuclei by cross-polarization[68] (CP) experiments.

NMR can also be used to probe domain sizes in heterogeneous solids.[69,70] In MAS DNP experiments, [1]H−[1]H spin diffusion usually distributes the proton hyperpolarization throughout the entire nuclear spin bath. We have recently shown how the dynamics of hyperpolarization in relayed-DNP experiments can be analyzed in terms of a polarization diffusion model to very efficiently extract domain sizes in active pharmaceuticals ingredients, microcrystalline solids and polymer blends.[71−73] Also, it is possible to measure the distance that polarization travels (from micrometer to nanometer scales), and determine layer structures, which has been shown in the case of organic crystalline nanoparticles[74] and lipid nanoparticle based drug delivery systems.[75]

Here, we characterize the transformations of poplar wood after different fractionation processes using relayed MAS DNP methods. We determine (i) the influence of the duration of the chemical treatment on the residual lignins; (ii) the role of dioxane and formaldehyde during chemical treatment; and (iii) that relayed DNP methods are regioselective toward the cell wall and distinguish the location of the residual lignins.

2. EXPERIMENTAL METHODS

2.1. Wood Sample Preparation. A transgenic plant, ferulate 5-hydroxylase downregulated poplar, was used as the wood sample in order to provide easily upgradeable and highly uniform lignin. Indeed, past studies have shown this lignin to be upgradeable at high yields (∼ 80%) and feature almost exclusively syringyl units (>98%; see structure in Scheme 1).[5,6] The sample was ball-milled into fine particles for 1 h using a PM100 planetary ball mill machine (Retsch, German) at 450 rpm. The ball-milled wood was placed in a thick wall glass reactor together with 9 mL of dioxane, 0.42 mL of 37% HCl, and 1 mL of a 36 wt % formaldehyde solution. The reactor was sealed tightly and placed in an oil bath at 80 °C for 0.5−2 h under continuous stirring. After the reaction, the mixture was filtered and the solid was washed with dioxane (3 × 5 mL). The residue was dried at 100 °C for 15 h. In the case where formaldehyde was not added during pretreatment, an extra 0.69 mL of H_2O was added to the reaction mixture. In the case where dioxane was not used during pretreatment, 10 mL of H_2O and 0.42 mL of 37% HCl were added instead of the aforementioned solution.

2.2. DNP Experiments. DNP experiments were performed on a 263 GHz/400 MHz AVANCE III Bruker DNP system. The spectrometer is equipped with a low temperature CPMAS probe and a 263 GHz gyrotron capable of outputting ca. 5−10 W of CW microwaves. The probe was configured in ^{1}H/^{13}C double mode. The sweep coil of the main magnetic field was optimized so that microwave irradiation gave the maximum positive proton DNP enhancement for AMUPol. DNP enhancements were determined by comparing the intensity of the spectra acquired with and without microwave irradiation, and the ^{1}H and ^{13}C enhancements are tabulated in the Supporting Information (SI) for all samples studied.

Note that all samples were ball milled at moderate conditions to maintain some fiber structure (as described above) and further ground in a mortar and pestle to obtain a homogeneous material before proceeding to DNP sample preparation.

For DNP experiments, typically 30 mg of ground wood sample was impregnated with 16 μL of 10 mM AMUPol in

D_2O/H_2O (9/1 v/v). The DNP sample was then packed in a 3.2 mm sapphire rotor and capped with a Teflon plug and zirconia cap. The filled DNP rotor was then spun at room temperature in the spinning station up to 12.5 kHz before being inserted into the precooled (ca. 100 K) 3.2 mm CPMAS DNP NMR probe, where the sample was frozen within several seconds.

2.3. DNP Enhanced ^1H and ^{13}C Solid-State NMR. For ^{13}C NMR experiments, the recycle delays were 3 or 4 s. The ^1H $\pi/2$ pulse length used for the variable amplitude CP experiments was 2.5 μs to afford 100 kHz ^1H decoupling using SPINAL-64.[76] The MAS frequency used is 12.5 kHz.

3. RESULTS AND DISCUSSION

3.1. ^{13}C NMR and DNP Enhanced NMR Features of Untreated Fibers. Figure 1A,B shows the conventional ^{13}C

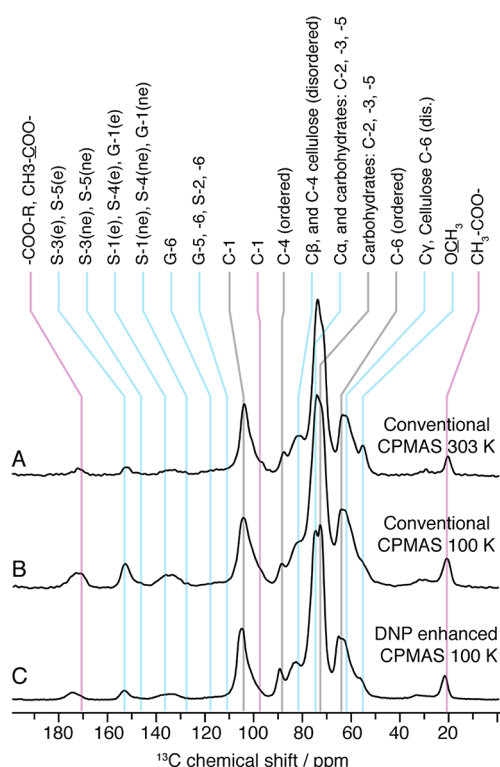**Figure 1.** ^{13}C CPMAS NMR spectra of untreated poplar wood acquired at (A) room temperature, 16 384 scans, 3 s recycle delay, 1 ms contact time, 12.5 kHz spinning rate and (B) at 100 K, 15 230 scans, 3 s recycle delay, 1 ms contact time, 12.5 kHz spinning rate. (C) ^{13}C CPMAS DNP enhanced NMR spectrum at 100 K, sample is impregnated with 10 mM AMUPol in D_2O/H_2O (9/1 v/v) 224 scans, 3 s recycle delay, 2 ms contact time, 12.5 Hz spinning rate. The assignment of the resonances follows the color code of the molecular structure of cellulose (black), hemicellulose (purple), and lignin (blue) described in Scheme 1. Abbreviations: ne is for nonetherified arylglycerol β-aryl ethers, and e indicates in etherified arylglycerol β-aryl ethers (see the SI for the table of chemical shifts).

CPMAS NMR spectra of untreated poplar wood recorded at room temperature (A) and at 100 K (B). Spectra A and B were acquired without DNP. Figure 1C shows the DNP enhanced ^{13}C CPMAS NMR spectrum of poplar wood impregnated with 10 mM AMUPol in D_2O/H_2O 9/1 v/v. The room temperature spectrum A is typical of lignocellulose and compares with all the data previously published.[8,9,77−80]

Full assignments of the main signals are shown in Figure 1 (chemical shifts are tabulated in the SI) and follow previous assignments of this type of material.[77,81] The identification of the main ^{13}C NMR resonances is important in order to follow the chemical changes of lignocellulosic materials during chemical and thermal treatment. The resonance at 21 ppm is assigned to the CH_3 carbons of the hemicelluloses acetate units. In the interval ranging between 60 and 105 ppm, large signals prevail which are predominantly assigned to cellulose, and to a lesser extent to hemicellulose carbohydrates. Of particular interest are the signals at 88.3 and 82.8 ppm, assigned to the C4 of cellulose allomorphs. The signal at 82.8 ppm is indicative of either amorphous or disordered cellulose at the surface of crystalline microfibers, whereas the signal at 88.3 ppm refers to crystalline cellulose.[81]

These signals overlap with the aliphatic carbons of lignins. In this area, the only resonance which can be specifically assigned to lignins is at 55.8 ppm, due to methoxy groups occurring in aromatic units. The intense signal 104.8 ppm is assigned to the C1 of cellulose, although some overlap with aromatic carbons of lignins cannot be excluded. A broad and weak shoulder centered at 102 ppm can be assigned to the C1 of hemicelluloses, with the broadness of this signal being clearly assigned to the amorphous structure. The peaks occurring in the region between 105 and 160 ppm are specific to carbons from the aromatic units of lignins. For hardwood, the presence of syringyl units is identified by the signal at 152.6 ppm classically assigned to C3 and C5 on the aromatic ring. On the low-frequency side of the previous signal, the shoulder is mainly assigned to the same carbons, but in nonetherified structures. The signal at 151.7 ppm is assigned to C1, and the signal at 148.4 can be assigned to C4 and C3 in guaiacyl units. The latter signal is quite weak, which is due to the low amounts of guaiacyl units in this type of transgenic poplar (<2%).[5] The shoulder at 144.1 ppm corresponds to C4 in nonetherified structures. The relative intensities of these two broad signals allow us to estimate the depletion of the lignin polymers in biomass materials. The signal at 172.6 ppm is generated by the carbonyls of hemicelluloses acetate groups.

Although the three spectra A−C were recorded under optimized experimental conditions, some differences are noticed. The first is a slight loss of resolution of the spectra recorded at low temperature (B and C) compared to the one recorded at room temperature (spectrum A). This is particularly visible for the signal of lignin methoxy and for the C4 of disordered celluloses and hemicelluloses. This is due to lignins and hemicelluloses being amorphous, and therefore, when their molecular dynamics become restrained at low temperatures, an increase in the NMR line widths is expected.[82] At low temperature, the lignin and hemicellulose become more rigid which explains an increase in their signal intensity for those regions of the spectra as CP will be more efficient.

As shown in the SI and summarized in Table S3, we compare the overall signal-to-noise ratio (SNR) of the DNP enhanced spectra to the conventional SSNMR spectra[83] for the untreated wood sample recorded at room temperature (RT) and at 100 K (both recorded on a dry powder without the addition of AMUPol solution). The ^{13}C SNR of the DNP enhanced spectra (acquired with microwave irradiation on) are 10 times that acquired without DNP at RT and 6 times higher than the spectrum acquired at 100 K, which represents a gain in experimental time of a factor 100 and 36, respectively. The

increase in intensity of the NMR signals observed at low temperature is expected and due to the Boltzmann factor. Note that, for the lignins and hemicelluloses, the gain in intensity is even larger, a factor 14 and 12, respectively (see SI Table S3).

3.2. Lignin Extraction. Pretreatment (or delignification) is a common process in biorefineries and pulp and the paper making industry. In a laboratory-scale method, lignin can be largely extracted using polar aprotic solvents such as dioxane under acidic conditions and elevated temperatures (>80 °C). We can use DNP enhanced NMR to follow the extent lignin extraction and the effect of the various pretreatment parameters on the biomass surface functionalities.

Figure 2 shows the ^{13}C CPMAS DNP enhanced NMR spectra of untreated poplar wood (F) as well as of poplar wood
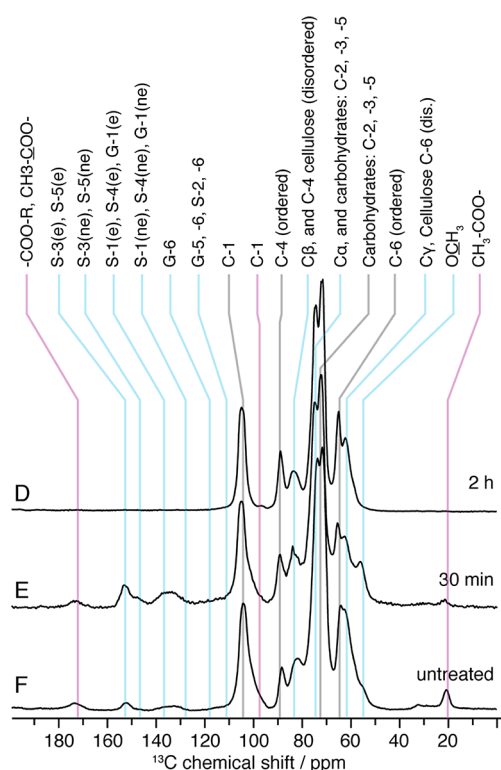

Figure 2. ^{13}C CPMAS DNP enhanced spectra of poplar wood treated with dioxane/H$_2$O/formaldehyde/HCl for 2 h (D) or 30 min (E), and untreated poplar wood (F), all impregnated with 10 mM AMUPol in D$_2$O/H$_2$O (9/1 v/v), where the spectra shown in the figure are normalized with respect to the intensity of the C1 peak of celluloses. The acquisition parameters for the spectra are as follows: spinning rate of 12.5 kHz, recycle delay of 3 s, and contact time of 1 ms, number of scans of 256 (D, F) and 1024 (E). Refer to Figure 1 for information on the color code and abbreviations.

after lignin extraction under acidic conditions with a dioxane/H$_2$O/formaldehyde solution for 30 min (E) or 2 h (D). The samples are all subsequently impregnated with 10 mM AMUPol in water (D$_2$O/H$_2$O 9/1 v/v). Scheme 2 illustrates a transverse section on the micrometer scale of the wood cell wall. We expect the radical solution to impregnate the cell lumen (CL) which is located at the exterior of the cell wall, and to also wet the layers of the secondary cell wall L3 and L2 (black and gray). The relative proportions of the three wood polymers (celluloses, hemicelluloses, and lignins) vary depending on the part of the cell wall. It is known that a greater

Scheme 2[a]
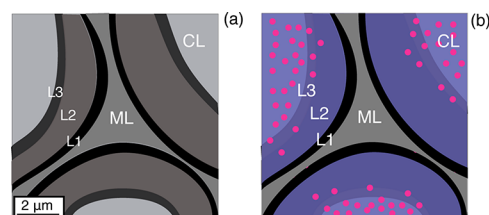
[a]Scheme of a transverse section of the wood cell wall at the μm scale (a) dry and (b) impregnated with radical solution (blue region) of AMUPol (pink circles) which depicts the cell lumen (CL) at the exterior of the cell walls, and the secondary cell wall layers (L3, L2, and L1). The radical solution should not reach the interior of the cell wall where the middle lamella (ML) is located.

concentration of lignins and hemicellulose is present in the middle lamella regions.[84]

On the basis of the assignments made previously, the interpretation of the changes observed in Figure 2 is straightforward. After 2 h of full treatment, we observe complete disappearance of both lignins and hemicelluloses (see Figure 2D). Note that for the residual celluloses the crystalline moiety is dominant as indicated by the signals assigned to C4 of crystalline and amorphous celluloses, respectively. There is no evidence of aromatic carbons. This means that, in the parts of the fibers of wood treated for 2 h which are accessible to DNP, the delignification can be considered almost complete. In contrast, when the pretreatment time was 30 min, the percentage of lignin appeared to increase within the solid residue as shown by the higher relative intensity of the lignin peaks (see Figure 2E). This increase could be explained by a biomass deconstruction mechanism where, in the initial 30 min of pretreatment, hemicellulose was the first to be removed while most of the lignin remained within the biomass matrix.

Furthermore, MAS DNP methods permit topological information about the depolymerization process to be obtained. In order to verify whether or not any residual lignin was still present inside the secondary layers of the cell wall, in particular in the deeper regions such as L1 and the middle lamella, the conventional ^{13}C CPMAS NMR spectrum of the sample of wood after full treatment for a period of 2 h, was recorded with 35 650 scans, and compared with a DNP enhanced spectrum recorded with 256 scans in Figure 3. The short broad peaks present at 130−160 ppm in the conventional spectrum indicated that small quantities of lignin remained within the solid residue. Whereas with the DNP enhanced spectrum, the aromatic region was quite clean, indicating almost no lignin was detected. This unambiguously indicates that the residual lignin is located in the interior of the cell wall, far from the DNP polarizing agent. A comparison of the signals intensities of residual D and G confirms that a very small amount of residual lignin (less that 4% of the total amount of carbon) remained inside the fiber.

3.3. Input of DNP Regioselectivity to Cell Wall. Figures 1 and S1 shows that the SNR of lignins (signals S-3(e), S-5(e) and S-1(e), S-4(e), G-1(e)) and hemicelluloses (−$\underline{C}$OO−R, CH$_3$−$\underline{C}$OO−, and $\underline{C}$H$_3$−COO−) decreases when impregnated with the radical solution (spectrum C, NO microwave irradiation) compared to the SSNMR spectrum B. The simplest explanation could be that lignins and hemicelluloses
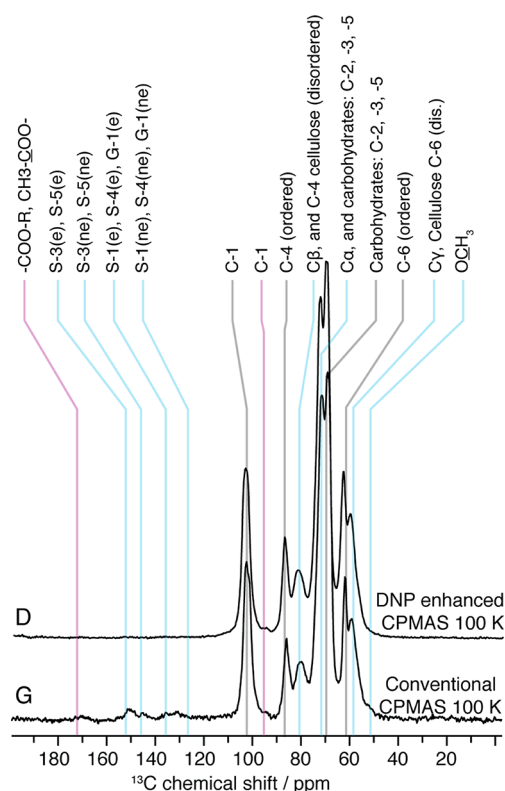
Figure 3. ^{13}C CPMAS NMR spectra acquired at 100 K of poplar wood treated with HCl for 2 h. Spectra are recorded at a spinning rate of 12 500 Hz, recycle delay of 3 s, and contact time of 1 ms. (D) DNP enhanced CPMAS NMR spectrum, sample impregnated with 10 mM AMUPol in D_2O/H_2O (9/1 v/v), 256 scans, and (G) conventional CPMAS NMR spectrum with 35 650 scans. The spectra are normalized with respect to the intensity of the C1 of celluloses. Refer to Figure 1 for information on the color code and abbreviations.

are more accessible to the biradical and that the signal is attenuated by bleaching effects.

Relaxation DNP experiments are used to determine the depolymerization process and to identify the components that remain inside the cell wall (see the SI for more details). Summarized in Table 1 are the experimental ^{1}H spin–lattice

Table 1. Measured ^{1}H Spin–Lattice Relaxation T_1 (s) at 100 K (Dry Sample) and for Wood Samples of Nontreated and Treated Wood (Full Treatment with and without Dioxane)^a

| | | treated 80 °C | | | |
| | | | | no dioxane | |
	nontreated	0.5 h	2 h	1 h	2 h
lignin	6.5	7.7	ND	0.85	1.3
cellulose	7.5	17.3	13.1	2.6	3.3
hemicellulose	7.0	7.3	ND	0.89	ND

^{a}ND: not determined because signal intensities were too weak.

relaxations (T_1) and in Table S4 are their corresponding diffusion lengths ($\rho_t = (D_t T_1)^{1/2}$) for treated and untreated (with or without dioxane) wood as determined from measurements of T_1, and assuming a constant spin diffusion coefficient (D_t) of 10^{-3} mm^2. s^{-1}.

The characteristic T_1 is longer for treated materials than for pristine wood which could be a consequence of the change in dynamics in the materials. If we consider the NMR signals

assigned to the cellulose moiety, all the lengths range between 80 and 130 nm for the treated and untreated samples (see Table in SI). The 80−130 nm range of diffusion lengths is clearly shorter than the total thickness expected for a lignocellulosic cell wall of wood materials which is on the order of 4−10 μm,[84−86] illustrating that the hyperpolarisation probes the surface of the cell walls. This confirms that MAS DNP enhances the secondary cell wall layers and allows a regioselective study of wood material. *This near surface characterization is of high relevance when working with chemical processes which are dependent upon the accessibility of the components involved in the process.*

As a result, direct interaction between lignins or hemicelluloses and AMUPol can be discarded, as these components are known to be more abundant in the deepest parts of the cell wall. Therefore the apparent loss of lignins and hemicelluloses observed above is due to the fact that the inner part of the cell wall, the middle lamella, is not observed by MAS DNP (see Scheme 2).

3.4. Role of Dioxane. Figures 4 and S2 show the spectra of the residues after being treated with an acidic aqueous solution (without dioxane) at different times and temperatures. The absence of dioxane leads to a strong accumulation of lignin in the cell lumen of the exterior cell wall. Several conclusions can
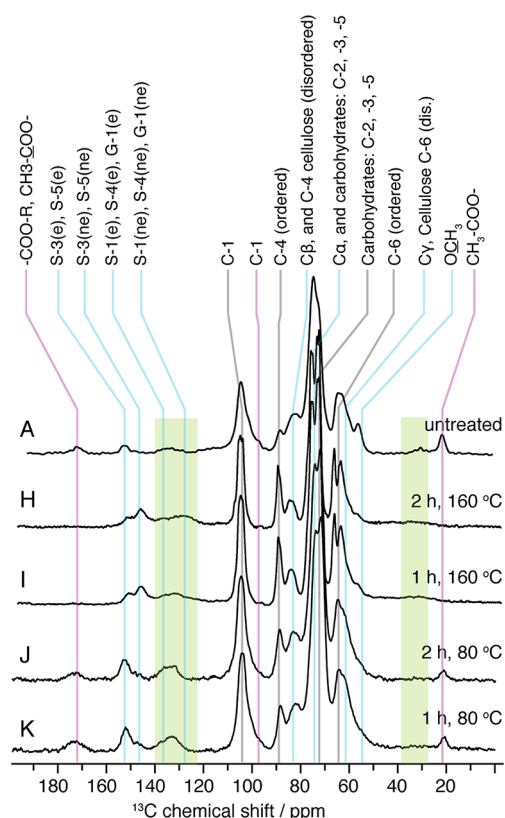

Figure 4. ^{13}C DNP enhanced CPMAS NMR spectra of poplar wood treated with the standard process (HCl) but without dioxane, acquired with a spinning rate of 12 500 Hz, recycle delays of 3 s, and contact time of 1 ms. Samples treated for (H) 2 h at 160 °C, 128 scans 128; (I) 1 h at 160 °C, 128 scans; (J) 2 h at 80 °C, 4 scans; (K) 1 h at 80 °C, 4 scans. The spectra are normalized with respect to the intensity of the C1 of celluloses. Refer to Figure 1 for information on the color code and abbreviations.

be drawn by comparing the lignin signals with those of the untreated wood (Figure 1A).

First, it appears that syringyl signals −3(ne), −5(ne) and guaiacyls −3(ne,e), −4(ne,e) strongly increase as the temperature increases from 80 to 160 °C. This indicates that the lignin was depolymerized, recondensed, and relocated on the surface of the fibers. These observations are consistent with an initial depolymerization of lignin, with β-O-4 cleavage, and subsequent repolymerization of said lignin on the surface of pretreated biomass, consistent with several literature reports.[87,88] Moreover, for the wood treated at 160 °C, either for 1 or 2 h, we observe depletion of acetyl groups and a new shoulder at 128 ppm and a broad signal centered at 33 ppm, which are not detectable in the samples treated at 80 °C. These signals are highlighted in green in Figure 4. Baccile et al. have assigned signals in this region to furan rings arising from the degradation of carbohydrates in the presence of water.[89] A possible explanation is that the carbohydrates (mainly hemicellulose in this case) were depolymerized under the acidic condition and partially converted into furans, which further condensed to humins on the cellulose surface. Due to the aforementioned regioselectivity of MAS DNP, we determine that the degradation products are formed within a 40 nm region from cell lumen and we can conclude that they correspond mainly to products that remain at the surface of the cell wall due to their insolubility in the absence of dioxane. In contrast, the spectrum of the sample pretreated with dioxane/HCl/H$_2$O/formaldehyde showed only peaks associated with carbohydrates. Thus, dioxane appears to greatly facilitate solubilization of lignin and hemicellulose derivatives during extraction, which prevents their reprecipitation on the surface. These controls were also run without formaldehyde which has also been shown to prevent condensation for both lignin and carbohydrates,[5,90] which likely further contributed to the absence of these residue signals when it was used.

3.5. Reaction of Formaldehyde on the Surface of Cellulose.

In order to gain a better understanding of the reactions between formaldehyde and biomass during lignin extraction, we used the ^{13}C labeled formaldehyde for the reaction and characterized the leftover solid after delignification to determine if the formaldehyde had reacted with any of the polysaccharide functionalities on the surface. With unlabeled formaldehyde (Figure 5N), no new ^{13}C NMR signals could indicate the occurrence of new structures between residual cellulose and formaldehyde, or self-polymerization, could be observed. Note that even under MAS DNP conditions no new signal were detected after 64 scans.

On the contrary, in the spectrum of Figure 5M of the material obtained using fully carbon-13 labeled formaldehyde, we clearly see new signals in the spectral range from 100 to 90 ppm and no significant changes in the cellulose resonances. They can be assigned to CH$_2$ in poly(oxymethylene) structures, as a result of self-polymerization of CH$_2$O inside the network of the remaining cell wall. Either way, the presence of this material at the surface explains the low activity that was previously observed during enzymatic hydrolysis of formaldehyde treated material. Either self-polymerized or covalently linked formaldehyde at the cellulose surface would block enzyme binding and reaction sites, which would lower hydrolysis activity.

The solid residue is mainly made of cellulose since lignins and hemicelluloses were almost completely depleted during extraction and dissolution in dioxane. The experiment using
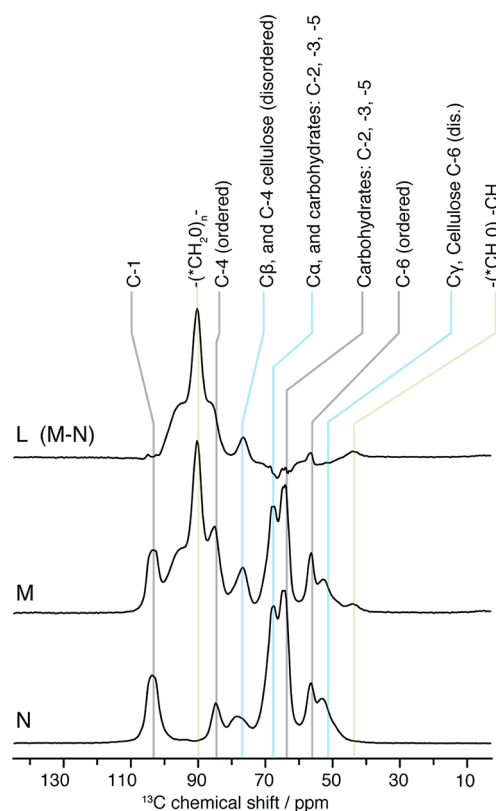

Figure 5. ^{13}C CPMAS DNP enhanced NMR spectra of poplar wood treated with the standard process of HCl for a period of 2 h at 80 °C using (M) labeled ^{13}C formaldehyde and (N) unlabeled ^{13}C formaldehyde. (L) is the difference spectrum between (M) and (N). All spectra were recorded with a spinning rate of 12 500 Hz, recycle delays of 3 s, contact time of 2.5 ms, and 64 scans. Refer to Figure 1 for information on the color code and abbreviations.

fully labeled ^{13}C formaldehyde permits one to quantify the amount of new structure formed with respect to the unlabeled sample. By comparison of the integral regions of the formaldehyde with respect to the integral of C1 of cellulose (see the spectrum in Figure S3), we obtained a ratio of 0.8 CHO per glucose unit. If we consider that formaldehyde is fully labeled (100%), the ratio has to be divided by the same factor to obtain a molar concentration of CHO per glucose units. It means that the sensitivity of NMR, even with DNP enhancement, remains in the range of 1%, within the corresponding surface. The depth of the considered surface corresponds to the diffusion distance. Considering the sample treated at 80 °C during 2 h which only shows cellulose signals (see spectrum D, Figure 2), the diffusion distance is equal to ~60 nm, which represents a depth of about six cellulose fibrils if we consider a cellulose fibril width of about 10 nm.

4. CONCLUSIONS

The high sensitivity of MAS DNP permits acquisition of ^{13}C solid-state NMR spectra in minutes. The carbon chemical shifts are good probes to distinguish between the various constituents of the poplar wood such as celluloses, hemicelluloses, and lignins. We have shown how MAS DNP methods allow the study of the topology resulting from pretreatment and fractionation processes of poplar wood where it clearly distinguishes between different sections of the wood cell wall. For example, lignin and hemicelluloses in

poplar wood were almost completely extracted after a 2 h pretreatment with dioxane/H_2O/formaldehyde/HCl according to the ^{13}C CPMAS spectrum. Shorter pretreatment process times of 30 min do not completely delignify poplar wood, as their residual signals are clearly observed in the ^{13}C CPMAS DNP enhanced NMR spectrum, but not in the conventional NMR spectrum. Hence, MAS DNP is a regioselective method to study wood materials. We show that polarization is effective in a 100 nm range for these wood materials.

We demonstrate that condensed lignins and humins which reprecipitated in the absence of dioxane and formaldehyde accumulated in a 40 nm external range of the cell wall. Finally, using fully enriched formaldehyde to follow the depolymerization mechanism with ^{13}C CPMAS NMR, we have demonstrated that 1% of the total amount of carbon on the surface of the material could be assigned to self-polymerization of the formaldehyde, which could explain previously observed reductions in cellulose digestibility by surface blockage.

■ ASSOCIATED CONTENT

ⓈSupporting Information

The Supporting Information is available free of charge at https://pubs.acs.org/doi/10.1021/acs.jpcc.9b09272.

> DNP enhanced NMR spectra, build-up curves, and numerical spin diffusion simulations (PDF)

■ AUTHOR INFORMATION

Corresponding Authors

*(J.L.) E-mail: jeremy.luterbacher@epfl.ch. Phone: +41 (0) 21 693 59 82.

*(M.B.) E-mail: michel.bardet@cea.fr. Phone: 33 (0)4 38 87 57 72. Fax: +33 (0)4 38 87 50 90.

ORCID 🄾

Pierrick Berruyer: 0000-0003-1783-6034

Lyndon Emsley: 0000-0003-1360-2572

Michel Bardet: 0000-0002-5628-2292

Jeremy Luterbacher: 0000-0002-0967-0583

Author Contributions

The manuscript was written through contributions of all authors. All authors have given approval to the final version of the manuscript.

Notes

The authors declare no competing financial interest.

■ ACKNOWLEDGMENTS

■ ABBREVIATIONS

DNP SENS, dynamic nuclear polarization surface enhanced spectroscopy; NMR, nuclear magnetic resonance; MAS, magic angle spinning; CP, cross-polarization; (S), syringyls; (G), guaiacyls; ne, nonetherified arylglycerol β-aryl ethers; e, etherified arylglycerol β-aryl ethers.

■ REFERENCES

(1) Sakellariou, P.; Rowe, R. C. Interactions in Cellulose Derivative Films for Oral-Drug Delivery. *Prog. Polym. Sci.* **1995**, *20*, 889−942.

(2) Klemm, D.; Heublein, B.; Fink, H. P.; Bohn, A. Cellulose: Fascinating Biopolymer and Sustainable Raw Material. *Angew. Chem., Int. Ed.* **2005**, *44*, 3358−3393.

(3) Moon, R. J.; Martini, A.; Nairn, J.; Simonsen, J.; Youngblood, J. Cellulose Nanomaterials Review: Structure, Properties and Nanocomposites. *Chem. Soc. Rev.* **2011**, *40*, 3941−3994.

(4) Zhu, H.; Luo, W.; Ciesielski, P. N.; Fang, Z.; Zhu, J. Y.; Henriksson, G.; Himmel, M. E.; Hu, L. Wood-Derived Materials for Green Electronics, Biological Devices, and Energy Applications. *Chem. Rev.* **2016**, *116*, 9305−74.

(5) Shuai, L.; Amiri, M. T.; Questell-Santiago, Y. M.; Héroguel, F.; Li, Y.; Kim, H.; Meilan, R.; Chapple, C.; Ralph, J.; Luterbacher, J. S. Formaldehyde Stabilization Facilitates Lignin Monomer Production During Biomass Depolymerization. *Science* **2016**, *354*, 329−333.

(6) Lan, W.; Amiri, M. T.; Hunston, C. M.; Luterbacher, J. S. Protection Group Effects During Alpha,Gamma-Diol Lignin Stabilization Promote High-Selectivity Monomer Production. *Angew. Chem., Int. Ed.* **2018**, *57*, 1356−1360.

(7) Talebi Amiri, M.; Dick, G. R.; Questell-Santiago, Y. M.; Luterbacher, J. S. Fractionation of Lignocellulosic Biomass to Produce Uncondensed Aldehyde-Stabilized Lignin. *Nat. Protoc.* **2019**, *14*, 921−954.

(8) Bardet, M.; Gagnaire, D.; Nardin, R.; Robert, D.; Vincendon, M. Use of C-13 Enriched Wood for Structural NMR Investigation of Wood and Wood Components, Cellulose and Lignins, in Solid and Liquid. *Holzforschung* **1986**, *40*, 17−24.

(9) Gil, A. M.; Neto, C. P. Solid-State NMR Studies of Wood and Other Lignocellulosic Materials. *Annu. Rep. NMR Spectrosc.* **1999**, *37*, 75−117.

(10) Melkior, T.; Jacob, S.; Gerbaud, G.; Hediger, S.; Le Pape, L.; Bonnefois, L.; Bardet, M. NMR Analysis of the Transformation of Wood Constituents by Torrefaction. *Fuel* **2012**, *92*, 271−280.

(11) Cheng, K.; Sorek, H.; Zimmermann, H.; Wemmer, D. E.; Pauly, M. Solution-State 2d N NMR mr Spectroscopy of Plant Cell Walls Enabled by a Dimethylsulfoxide-D6/1-Ethyl-3-Methylimidazolium Acetate Solvent. *Anal. Chem.* **2013**, *85*, 3213−21.

(12) Terashima, N.; Kitano, K.; Kojima, M.; Yoshida, M.; Yamamoto, H.; Westermark, U. Nanostructural Assembly of Cellulose, Hemicellulose, and Lignin in the Middle Layer of Secondary Wall of Ginkgo Tracheid. *J. Wood Sci.* **2009**, *55*, 409−416.

(13) Yelle, D. J.; Ralph, J.; Frihart, C. R. Characterization of Nonderivatized Plant Cell Walls Using High-Resolution Solution-State Nm NMR r Spectroscopy. *Magn. Reson. Chem.* **2008**, *46*, 508−517.

(14) Mansfield, S. D.; Kim, H.; Lu, F.; Ralph, J. Whole Plant Cell Wall Characterization Using Solution-State 2D NMR. *Nat. Protoc.* **2012**, *7*, 1579−89.

(15) Kim, H.; Ralph, J. A Gel-State 2D-NMR Method for Plant Cell Wall Profiling and Analysis: A Model Study with the Amorphous Cellulose and Xylan from Ball-Milled Cotton Linters. *RSC Adv.* **2014**, *4*, 7549−7560.

(16) Kim, H.; Ralph, J. Solution-State 2d NMR of Ball-Milled Plant Cell Wall Gels in DMSO-D6/Pyridine-D5. *Org. Biomol. Chem.* **2010**, *8*, 576−591.

(17) Bardet, M.; Gerbaud, G.; Doan, C.; Giffard, M.; Hediger, S.; De Paepe, G.; Tran, Q. K. Dynamics Property Recovery of Archaeological-Wood Fibers Treated with Polyethylene Glycol Demonstrated by High-Resolution Solid-State NMR. *Cellulose* **2012**, *19*, 1537−1545.

(18) Simmons, T. J.; Mortimer, J. C.; Bernardinelli, O. D.; Poppler, A. C.; Brown, S. P.; Deazevedo, E. R.; Dupree, R.; Dupree, P. Folding of Xylan onto Cellulose Fibrils in Plant Cell Walls Revealed by Solid-State NMR. *Nat. Commun.* **2016**, *7*, 13902.

(19) Kang, X.; Kirui, A.; Dickwella Widanage, M. C.; Mentink-Vigier, F.; Cosgrove, D. J.; Wang, T. Lignin-Polysaccharide Interactions in Plant Secondary Cell Walls Revealed by Solid-State NMR. *Nat. Commun.* **2019**, *10*, 347.

(20) Grantham, N. J.; et al. An Even Pattern of Xylan Substitution Is Critical for Interaction with Cellulose in Plant Cell Walls. *Nature Plants* **2017**, *3*, 859–865.

(21) Dupree, R.; Simmons, T. J.; Mortimer, J. C.; Patel, D.; Iuga, D.; Brown, S. P.; Dupree, P. Probing the Molecular Architecture of Arabidopsis Thaliana Secondary Cell Walls Using Two- and Three-Dimensional ^{13}C Solid State Nuclear Magnetic Resonance Spectroscopy. *Biochemistry* **2015**, *54*, 2335–45.

(22) Wickholm, K.; Larson, P. T.; Iversen, T. Assignment of Non-Crystalline Forms in Cellulose I by CP/MAS ^{13}C NMR Spectroscopy. *Carbohydr. Res.* **1998**, *312*, 123–129.

(23) Atalla, R. H.; VanderHart, D. L. The Role of Solid State ^{13}C NMR Spectroscopy in Studies of the Nature of Native Cellulose. *Solid State Nucl. Magn. Reson.* **1999**, *15*, 1–19.

(24) Dick-Perez, M.; Zhang, Y.; Hayes, J.; Salazar, A.; Zabotina, O. A.; Hong, M. Structure and Interactions of Plant Cell-Wall Polysaccharides by Two- and Three-Dimensional Magic-Angle-Spinning Solid-State NMR. *Biochemistry* **2011**, *50*, 989–1000.

(25) Foston, M. Advances in Solid-State NMR of Cellulose. *Curr. Opin. Biotechnol.* **2014**, *27*, 176–84.

(26) Masuda, K.; Adachi, M.; Hirai, A.; Yamamoto, H.; Kaji, H.; Horii, F. Solid-State ^{13}C and ^{1}H Spin Diffusion NMR Analyses of the Microfibril Structure for Bacterial Cellulose. *Solid State Nucl. Magn. Reson.* **2003**, *23*, 198–212.

(27) Ni, Q. Z.; Daviso, E.; Can, T. V.; Markhasin, E.; Jawla, S. K.; Swager, T. M.; Temkin, R. J.; Herzfeld, J.; Griffin, R. G. High Frequency Dynamic Nuclear Polarization. *Acc. Chem. Res.* **2013**, *46*, 1933–1941.

(28) Rossini, A. J.; Zagdoun, A.; Lelli, M.; Lesage, A.; Copéret, C.; Emsley, L. Dynamic Nuclear Polarization Surface Enhanced NMR Spectroscopy. *Acc. Chem. Res.* **2013**, *46*, 1942–1951.

(29) Lesage, A.; et al. Surface Enhanced NMR Spectroscopy by Dynamic Nuclear Polarization. *J. Am. Chem. Soc.* **2010**, *132*, 15459–15461.

(30) Love, A. M. Probing the Transformation of Boron Nitride Catalysts under Oxidative Dehydrogenation Conditions. *J. Am. Chem. Soc.* **2019**, *141*, 182.

(31) Walder, B. J.; Berk, C.; Liao, W. C.; Rossini, A. J.; Schwarzwalder, M.; Pradere, U.; Hall, J.; Lesage, A.; Coperet, C.; Emsley, L. One- and Two-Dimensional High-Resolution NMR from Flat Surfaces. *ACS Cent. Sci.* **2019**, *5*, 515–523.

(32) Piveteau, L.; et al. Resolving the Core and the Surface of Cdse Quantum Dots and Nanoplatelets Using Dynamic Nuclear Polarization Enhanced PASS–PIETA NMR Spectroscopy. *ACS Cent. Sci.* **2018**, *4*, 1113–1125.

(33) Hope, M. A.; Halat, D. M.; Magusin, P. C.; Paul, S.; Peng, L.; Grey, C. P. Surface-Selective Direct 17O DNP NMR of CeO2 Nanoparticles. *Chem. Commun.* **2017**, *53*, 2142–2145.

(34) Wolf, T.; Kumar, S.; Singh, H.; Chakrabarty, T.; Aussenac, F.; Frenkel, A. I.; Major, D. T.; Leskes, M. Endogenous Dynamic Nuclear Polarization for Natural Abundance ^{17}O and Lithium NMR in the Bulk of Inorganic Solids. *J. Am. Chem. Soc.* **2019**, *141*, 451–462.

(35) Mais, M.; Torroba, J.; Barrow, N. S.; Paul, S.; Titman, J. J. Ion Exchange and Binding in Selenium Remediation Materials Using DNP-Enhanced Solid-State NMR Spectroscopy. *Solid State Nucl. Magn. Reson.* **2019**, *98*, 19–23.

(36) Bjorgvinsdottir, S.; Walder, B. J.; Pinon, A. C.; Emsley, L. Bulk Nuclear Hyperpolarization of Inorganic Solids by Relay from the Surface. *J. Am. Chem. Soc.* **2018**, *140*, 7946–7951.

(37) Pump, E.; et al. Predicting the DNP-Sens Efficiency in Reactive Heterogeneous Catalysts from Hydrophilicity. *Chem. Sci.* **2018**, *9*, 4866–4872.

(38) Kobayashi, T.; Perras, F. A.; Slowing, I. I.; Sadow, A. D.; Pruski, M. Dynamic Nuclear Polarization Solid-State NMR in Heterogeneous Catalysis Research. *ACS Catal.* **2015**, *5*, 7055–7062.

(39) Rankin, A. G. M.; Webb, P. B.; Dawson, D. M.; Viger-Gravel, J.; Walder, B. J.; Emsley, L.; Ashbrook, S. E. Determining the Surface Structure of Silicated Alumina Catalysts Via Isotopic Enrichment and Dynamic Nuclear Polarization Surface-Enhanced NMR Spectroscopy. *J. Phys. Chem. C* **2017**, *121*, 22977–22984.

(40) Moroz, I. B.; Larmier, K.; Liao, W.-C.; Copéret, C. Discerning Γ-Alumina Surface Sites with Nitrogen-15 Dynamic Nuclear Polarization Surface Enhanced NMR Spectroscopy of Adsorbed Pyridine. *J. Phys. Chem. C* **2018**, *122*, 10871–10882.

(41) Leskes, M.; Kim, G.; Liu, T.; Michan, A. L.; Aussenac, F.; Dorffer, P.; Paul, S.; Grey, C. P. Surface-Sensitive NMR Detection of the Solid Electrolyte Interphase Layer on Reduced Graphene Oxide. *J. Phys. Chem. Lett.* **2017**, *8*, 1078–1085.

(42) Berruyer, P.; Lelli, M.; Conley, M. P.; Silverio, D. L.; Widdifield, C. M.; Siddiqi, G.; Gajan, D.; Lesage, A.; Coperet, C.; Emsley, L. Three-Dimensional Structure Determination of Surface Sites. *J. Am. Chem. Soc.* **2017**, *139*, 849–855.

(43) Kumar, A.; Walder, B. J.; Kunhi Mohamed, A.; Hofstetter, A.; Srinivasan, B.; Rossini, A. J.; Scrivener, K.; Emsley, L.; Bowen, P. The Atomic-Level Structure of Cementitious Calcium Silicate Hydrate. *J. Phys. Chem. C* **2017**, *121*, 17188–17196.

(44) Sangodkar, R. P.; Smith, B. J.; Gajan, D.; Rossini, A. J.; Roberts, L. R.; Funkhouser, G. P.; Lesage, A.; Emsley, L.; Chmelka, B. F. Influences of Dilute Organic Adsorbates on the Hydration of Low-Surface-Area Silicates. *J. Am. Chem. Soc.* **2015**, *137*, 8096–112.

(45) Ouari, O.; Phan, T.; Ziarelli, F.; Casano, G.; Aussenac, F.; Thureau, P.; Gigmes, D.; Tordo, P.; Viel, S. Improved Structural Elucidation of Synthetic Polymers by Dynamic Nuclear Polarization Solid-State NMR Spectroscopy. *ACS Macro Lett.* **2013**, *2*, 715–719.

(46) Mollica, G.; et al. Observing Apparent Nonuniform Sensitivity Enhancements in Dynamic Nuclear Polarization Solid-State NMR Spectra of Polymers. *ACS Macro Lett.* **2014**, *3*, 922–925.

(47) Le, D.; et al. Optimizing Sample Preparation Methods for Dynamic Nuclear Polarization Solid-State NMR of Synthetic Polymers. *Macromolecules* **2014**, *47*, 3909–3916.

(48) Verde-Sesto, E.; Goujon, N.; Sardon, H.; Ruiz, P.; Huynh, T. V.; Elizalde, F.; Mecerreyes, D.; Forsyth, M.; O'Dell, L. A. DNP NMR Studies of Crystalline Polymer Domains by Copolymerization with Nitroxide Radical Monomers. *Macromolecules* **2018**, *51*, 8046–8053.

(49) Schäfer, T.; Vowinkel, S.; Breitzke, H.; Gallei, M.; Gutmann, T. Selective DNP Signal Amplification to Probe Structures of Core–Shell Polymer Hybrid Nanoparticles. *J. Phys. Chem. C* **2019**, *123*, 644–652.

(50) Smith, A. N.; Long, J. R. Dynamic Nuclear Polarization as an Enabling Technology for Solid State Nuclear Magnetic Resonance Spectroscopy. *Anal. Chem.* **2016**, *88*, 122–32.

(51) Gupta, R.; et al. Dynamic Nuclear Polarization Enhanced MAS NMR Spectroscopy for Structural Analysis of Hiv-1 Protein Assemblies. *J. Phys. Chem. B* **2016**, *120*, 329–39.

(52) Jaudzems, K.; et al. Dynamic Nuclear Polarization-Enhanced Biomolecular NMR Spectroscopy at High Magnetic Field with Fast Magic-Angle Spinning. *Angew. Chem., Int. Ed.* **2018**, *57*, 7458–7462.

(53) Ni, Q. Z.; Daviso, E.; Can, T. V.; Markhasin, E.; Jawla, S. K.; Swager, T. M.; Temkin, R. J.; Herzfeld, J.; Griffin, R. G. *Acc. Chem. Res.* **2013**, *46*, 1933–1941.

(54) Ni, Q. Z.; Can, T. V.; Daviso, E.; Belenky, M.; Griffin, R. G.; Herzfeld, J. Primary Transfer Step in the Light-Driven Ion Pump Bacteriorhodopsin: An Irreversible U-Turn Revealed by Dynamic Nuclear Polarization-Enhanced Magic Angle Spinning NMR. *J. Am. Chem. Soc.* **2018**, *140*, 4085–4091.

(55) Marin-Montesinos, I.; Goyard, D.; Gillon, E.; Renaudet, O.; Imberty, A.; Hediger, S.; De Paëpe, G. Selective High-Resolution DNP-Enhanced NMR of Biomolecular Binding Sites. *Chem. Sci.* **2019**, *10*, 3366.

(56) Ni, Q. Z.; et al. In Situ Characterization of Pharmaceutical Formulations by Dynamic Nuclear Polarization Enhanced MAS NMR. *J. Phys. Chem. B* **2017**, *121*, 8132–8141.

(57) Hirsh, D. A.; Rossini, A. J.; Emsley, L.; Schurko, R. W. (35)Cl Dynamic Nuclear Polarization Solid-State NMR of Active Pharmaceutical Ingredients. *Phys. Chem. Chem. Phys.* **2016**, *18*, 25893–25904.

(58) Zhao, L.; Hanrahan, M. P.; Chakravarty, P.; DiPasquale, A. G.; Sirois, L. E.; Nagapudi, K.; Lubach, J. W.; Rossini, A. J.

Characterization of Pharmaceutical Cocrystals and Salts by Dynamic Nuclear Polarization-Enhanced Solid-State NMR Spectroscopy. *Cryst. Growth Des.* **2018**, *18*, 2588−2601.

(59) Zhao, L.; Pinon, A. C.; Emsley, L.; Rossini, A. J. DNP-Enhanced Solid-State NMR Spectroscopy of Active Pharmaceutical Ingredients. *Magn. Reson. Chem.* **2018**, *56*, 583−609.

(60) Takahashi, H.; Lee, D.; Dubois, L.; Bardet, M.; Hediger, S.; De Paepe, G. Rapid Natural-Abundance 2D C-13-C-13 Correlation Spectroscopy Using Dynamic Nuclear Polarization Enhanced Solid-State Nmr and Matrix-Free Sample Preparation. *Angew. Chem., Int. Ed.* **2012**, *51*, 11766−11769.

(61) Wang, T.; Park, Y. B.; Caporini, M. A.; Rosay, M.; Zhong, L.; Cosgrove, D. J.; Hong, M. Sensitivity-Enhanced Solid-State NMR Detection of Expansin's Target in Plant Cell Walls. *Proc. Natl. Acad. Sci. U. S. A.* **2013**, *110*, 16444−9.

(62) Perras, F. A.; Luo, H.; Zhang, X.; Mosier, N. S.; Pruski, M.; Abu-Omar, M. M. Atomic-Level Structure Characterization of Biomass Pre- and Post-Lignin Treatment by Dynamic Nuclear Polarization-Enhanced Solid-State NMR. *J. Phys. Chem. A* **2017**, *121*, 623−630.

(63) Gutmann, T.; Kumari, B.; Zhao, L.; Breitzke, H.; Schoettner, S.; Ruettiger, C.; Gallei, M. Dynamic Nuclear Polarization Signal Amplification as a Sensitive Probe for Specific Functionalization of Complex Paper Substrates. *J. Phys. Chem. C* **2017**, *121*, 3896−3903.

(64) Sauvee, C.; Rosay, M.; Casano, G.; Aussenac, F.; Weber, R. T.; Ouari, O.; Tordo, P. Highly Efficient, Water-Soluble Polarizing Agents for Dynamic Nuclear Polarization at High Frequency. *Angew. Chem., Int. Ed.* **2013**, *52*, 10858−61.

(65) Song, C.; Hu, K.-N.; Joo, C.-G.; Swager, T. M.; Griffin, R. G. Totapol: A Biradical Polarizing Agent for Dynamic Nuclear Polarization Experiments in Aqueous Media. *J. Am. Chem. Soc.* **2006**, *128*, 11385−11390.

(66) Kubicki, D. J.; et al. Rational Design of Dinitroxide Biradicals for Efficient Cross-Effect Dynamic Nuclear Polarization. *Chem. Sci.* **2016**, *7*, 550−558.

(67) Zagdoun, A.; et al. Large Molecular Weight Nitroxide Biradicals Providing Efficient Dynamic Nuclear Polarization at Temperatures up to 200 K. *J. Am. Chem. Soc.* **2013**, *135*, 12790−12797.

(68) Pines, A.; Gibby, M. G.; Waugh, J. S. Proton-Enhanced Nuclear Induction Spectroscopy. A Method for High Resolution NMR of Dilute Spins in Solids. *J. Chem. Phys.* **1972**, *56*, 1776−1777.

(69) Demco, D. E.; Johansson, A.; Tegenfeldt, J. Proton Spin Diffusion for Spatial Heterogeneity and Morphology Investigations of Polymers. *Solid State Nucl. Magn. Reson.* **1995**, *4*, 13−38.

(70) Clauss, J.; Schmidt-Rohr, K.; Spiess, H. W. Determination of Domain Sizes in Heterogeneous Polymers by Solid-State NMR. *Acta Polym.* **1993**, *44*, 1−17.

(71) Rossini, A. J.; Widdifield, C. M.; Zagdoun, A.; Lelli, M.; Schwarzwalder, M.; Coperet, C.; Lesage, A.; Emsley, L. Dynamic Nuclear Polarization Enhanced NMR Spectroscopy for Pharmaceutical Formulations. *J. Am. Chem. Soc.* **2014**, *136*, 2324−2334.

(72) Pinon, A. C.; et al. Measuring Nano- to Microstructures from Relayed Dynamic Nuclear Polarization NMR. *J. Phys. Chem. C* **2017**, *121*, 15993−16005.

(73) Schlagnitweit, J.; Tang, M.; Baias, M.; Richardson, S.; Schantz, S.; Emsley, L. Nanostructure of Materials Determined by Relayed Paramagnetic Relaxation Enhancement. *J. Am. Chem. Soc.* **2015**, *137*, 12482−12485.

(74) Pinon, A. C.; Skantze, U.; Viger-Gravel, J.; Schantz, S.; Emsley, L. Core-Shell Structure of Organic Crystalline Nanoparticles Determined by Relayed Dynamic Nuclear Polarization NMR. *J. Phys. Chem. A* **2018**, *122*, 8802−8807.

(75) Viger-Gravel, J.; Schantz, A.; Pinon, A. C.; Rossini, A. J.; Schantz, S.; Emsley, L. Structure of Lipid Nanoparticles Containing Sirna or Mrna by Dynamic Nuclear Polarization-Enhanced NMR Spectroscopy. *J. Phys. Chem. B* **2018**, *122*, 2073−2081.

(76) Fung, B. M.; Khitrin, A. K.; Ermolaev, K. *J. Magn. Reson.* **2000**, *142*, 97.

(77) Bardet, M.; Emsley, L.; Vincendon, M. Two-Dimensional Spin-Exchange Solid-State NMR Studies of C-13-Enriched Wood. *Solid State Nucl. Magn. Reson.* **1997**, *8*, 25−32.

(78) Lesage, A.; Bardet, M.; Emsley, L. Through-Bond Carbon-Carbon Connectivities in Disordered Solids by NMR. *J. Am. Chem. Soc.* **1999**, *121*, 10987−10993.

(79) Bardet, M.; Hediger, S.; Gerbaud, G.; Gambarelli, S.; Jacquot, J. F.; Foray, M. F.; Gadelle, A. Investigation with C-13 NMR, EPR and Magnetic Susceptibility Measurements of Char Residues Obtained by Pyrolysis of Biomass. *Fuel* **2007**, *86*, 1966−1976.

(80) Melkior, T.; Barthomeuf, C.; Bardet, M. Inputs of Solid-State NMR to Evaluate and Compare Thermal Reactivity of Pine and Beech Woods under Torrefaction Conditions and Modified Atmosphere. *Fuel* **2017**, *187*, 250−260.

(81) Bardet, M.; Gerbaud, G.; Giffard, M.; Doan, C.; Hediger, S.; Pape, L. L. ^{13}C High-Resolution Solid-State NMR for Structural Elucidation of Archaeological Woods. *Prog. Nucl. Magn. Reson. Spectrosc.* **2009**, *55*, 199−214.

(82) Lewandowski, J. R.; Halse, M. E.; Blackledge, M.; Emsley, L. Direct Observation of Hierarchical Protein Dynamics. *Science* **2015**, *348*, 578−581.

(83) Rossini, A. J.; Zagdoun, A.; Lelli, M.; Gajan, D.; Rascón, F.; Rosay, M.; Maas, W. E.; Copéret, C.; Lesage, A.; Emsley, L. One Hundred Fold Overall Sensitivity Enhancements for Silicon-29 NMR Spectroscopy of Surfaces by Dynamic Nuclear Polarization with CPMG Acquisition. *Chem. Sci.* **2012**, *3*, 108−115.

(84) Sorieul, M.; Dickson, A.; Hill, S. J.; Pearson, H. Plant Fibre: Molecular Structure and Biomechanical Properties, of a Complex Living Material, Influencing Its Deconstruction Towards a Biobased Composite. *Materials* **2016**, *9*, 618−643.

(85) Fahlen, J.; Salmen, L. Cross-Sectional Structure of the Secondary Wall of Wood Fibers as Affected by Processing. *J. Mater. Sci.* **2003**, *38*, 119−126.

(86) Reza, M.; Kontturi, E.; Jaaskelainen, A. S.; Vuorinen, T.; Ruokolainen, J. Transmission Electron Microscopy for Wood and Fiber Analysis - a Review. *Bioresources* **2015**, *10*, 6230−6261.

(87) Selig, M.J.; Viamajala, S.; Decker, S.R.; Tucker, M.P.; Himmel, M.E.; Vinzant, T.B. Deposition of Lignin Droplets Produced During Dilute Acid Pretreatment of Maize Stems Retards Enzymatic Hydrolysis of Cellulose. *Biotechnol. Prog.* **2007**, *23*, 1333−1339.

(88) Pielhop, T.; Larrazábal, G. O.; Studer, M. H.; Brethauer, S.; Seidel, C.-M.; Rudolf von Rohr, P. Lignin Repolymerisation in Spruce Autohydrolysis Pretreatment Increases Cellulase Deactivation. *Green Chem.* **2015**, *17*, 3521−3532.

(89) Baccile, N.; Laurent, G.; Babonneau, F.; Fayon, F.; Titirici, M. M.; Antonietti, M. Structural Characterization of Hydrothermal Carbon Spheres by Advanced Solid-State MAS ^{13}C NMR Investigations. *J. Phys. Chem. C* **2009**, *113*, 9644−9654.

(90) Questell-Santiago, Y. M.; Zambrano-Varela, R.; Talebi Amiri, M.; Luterbacher, J. S. Carbohydrate Stabilization Extends the Kinetic Limits of Chemical Polysaccharide Depolymerization. *Nat. Chem.* **2018**, *10*, 1222−1228.